BG#: 2396
Article#: 98.113
Typesetter: sab
Artist: mb
Editor: db

Nanoscale heterogeneities in amorphous semiconductor$_x$ metal$_{1-x}$ alloys: A small-angle x-ray scattering study

J. S. Rigden and R. J. Newport[a)]
School of Physical Sciences, The University, Canterbury, Kent, CT2 7NR, United Kingdom

(Received 13 March 1998; accepted 2 September 1998)

A series of small-angle x-ray scattering (SAXS) experiments has been conducted in order to probe further the X-ray absorption fine structure (EXAFS)-derived nanoscale structure of amorphous hydrogenated silicon$_x$tin$_{1-x}$, hydrogenated silicon$_x$nickel$_{1-x}$, and germanium$_x$gold$_{1-x}$ materials as a function of metal content. The SAXS results reveal information on cluster formation within these reactively radio-frequency–sputtered amorphous thin films. The data are considered within the context of EXAFS data, and lend support to a model in which the degree and nature of the heterogeneities depend primarily on the metal species, with the level of metal content inducing additional effects. In particular, the results support a percolation model for the metal : nonmetal transition in amorphous semiconductor$_x$transition metal$_{1-x}$ alloys, the conducting volume elements comprising metal, or metal compound-rich regions within the amorphous tetrahedral host network.

I. INTRODUCTION

Noncrystalline semiconductors are of immense technological interest, having many and varied applications. Of fundamental significance are materials formed by alloying amorphous hydrogenated silicon, *a*-Si : H with metals (M); by careful control of the composition of the materials formed (*a*-Si$_x$M$_{1-x}$: H), it is possible to regulate the electrical conductivity and for certain metal impurities, e.g., noble and transition metals, to induce a transition from semiconducting to metallic-type behavior above a certain critical limit. The electronic properties of such alloys have been extensively studied[1] and the metal : insulator transitions (MIT) are often described in terms of an Anderson-type transition where electrons at the Fermi level become delocalized and extended state conduction can occur. However, this approach relies on the assumption that the impurity atoms are incorporated randomly into the structure. If clustering of metal atoms occurs, it is more appropriate to describe the electrical conductivity in terms of classical percolation theory.[2]

In contrast to the behavior described above, alloying *a*-Si : H with the group IV element, tin, does not induce an MIT transition as such. As the metal concentration is increased, the optical bandgap smoothly decreases along with a concomitant increase in dark conductivity.[3] However, above approximately 5 at.% Sn, the conduction process changes from *n*-type to *p*-type and the photoconductivity falls.[4] This latter phenomenon has been attributed to the nonsubstitutional inclusion of impurity atoms.

It is evident that, to clarify our understanding of the conductivity processes in *a*-Si$_x$M$_{1-x}$ systems, it would be advantageous to have a knowledge of the atomic scale structure of the materials and the way in which the impurity atoms are included in the tetrahedral random network (TRN) of the host semiconductor. To this end we investigated the structure of three alloy systems of interest (*a*-Si$_x$Ni$_{1-x}$: H,[5] *a*-Ge$_x$Au$_{1-x}$,[6] and *a*-Si$_x$Sn$_{1-x}$: H;[7] see also Refs. 8 and 9) over pertinent composition ranges using the technique of extended x-ray absorption fine structure (EXAFS).

Broadly speaking, our conclusion was that the inclusion of Ni into *a*-Si and Au into *a*-Ge leads to local reordering of the TRN. It was suggested that small regions of intermetallic compound are formed and are surrounded by the matrix provided by the persisting amorphous semiconductor; the systems are therefore, within this model, heterogeneous. More specifically, we suggested that clusters of a highly disordered form of intermetallic $NiSi_2$ were formed in *a*-Si$_x$Ni$_{1-x}$: H, and analogous (metastable) clusters of $Au_{60}Ge_{40}$ in the *a*-Ge$_x$Au$_{1-x}$. Indeed, there is some evidence for the additional formation of metallic gold clusters at higher Au concentrations. Certainly, if this picture is at all realistic it would imply that a percolation model would be the most appropriate basis for a description of the transport behavior. No such evidence for segregation exists for the *a*-Si$_x$Sn$_{1-x}$: H system, but rather the EXAFS data supported a random substitutional model. Studies on the nature of the conductivity and magnetoresistance of *a*-Si$_x$Ni$_{1-x}$: H near the MIT[10] lend further support to our

a)Address correspondence to this author.
e-mail: r.j.newport@ukc.ac.uk

proposed structural model. In an EXAFS study[11] that revisits the earlier experiments in part, data is presented for relatively high nickel concentrations; this additional data shows rather similar features to our initial study. The authors, however, quite justifiably, highlight the fact that from EXAFS data alone it is not possible to make an unambiguous statement on the nature of the systems' structures beyond near-neighbors. This obvious point reflects one of the intrinsic limitations of the EXAFS technique, and it is with this in mind that we now present the results of a complementary study using small angle x-ray scattering (SAXS).

II. SAMPLE PREPARATION

Thin film samples of thickness approximately 2 μm were deposited onto mylar substrates, which were held at ambient temperature, by reactive cosputtering. Argon (99.998% purity) was used as the sputtering gas with H_2 (99.993% purity) added in the ratio 10/1, Ar/H_2, to saturate dangling bonds in the samples. The total pressure was 7.3×10^{-3} mbar with a constant rf power of 200 W and a target bias of $\sim$700 V. The composition of the samples was controlled by varying the number of small metal disks arranged on the 10 cm diameter crystalline semiconductor target to give a homogeneous distribution at the substrate. However, the a-Ge$_x$Au$_{1-x}$ samples were not hydrogenated to aid qualitative comparison with previous work on this system. Compositional analysis was initially performed using an electron microprobe but later refined significantly using α-particle Rutherford backscattering. Each sample was also found to contain an approximately constant proportion (8 at.%) of Ar incorporated during the sputtering process; the Ar sites have been shown to be randomly distributed within the TRN and to have no discernible effect on the overall network structure.[9] The amount of hydrogen incorporated in the hydrogenated samples was not quantitatively evaluated; however, infrared absorption spectroscopy shows the presence of Si–H bonds at all compositions, and work on analogous materials (e.g., Ref. 18) suggests a total H content of $\sim$10 at.%.

III. SAXS EXPERIMENTATION AND DATA REDUCTION

Small-angle x-ray scattering data was collected on Station 8.2 at the Synchrotron Radiation Source at CCRL Daresbury Laboratory, UK. SAXS is a nondestructive method for examining structure in the size range $\sim$10 to a few 100 Å, and the principles are detailed elsewhere.[12] The main components of the SAXS setup are presented in Fig. 1. X-rays, monochromated by an arrangement of optics, are incident on the sample and scattered to a range of angles θ. Variations in the incident beam intensity, and the transmittance

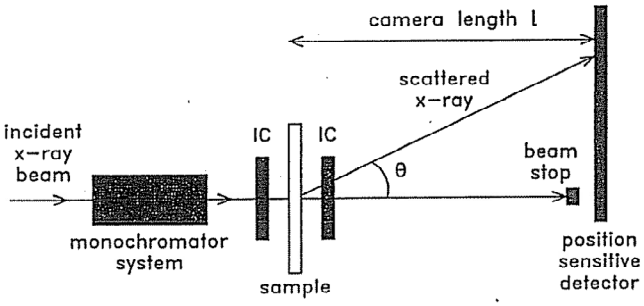

FIG. 1. Schematic diagram of the SAXS arrangement.

of the sample, are monitored using the ionization chambers, labelled *IC* in the figure. The scattered radiation travels down an evacuated camera and is incident on a position sensitive detector at a distance l from the sample; a beam stop is used to absorb the straight-through beam which would otherwise damage the detector. The length of the camera determines the range of scattering angles subtended by the detector; this can be chosen to span a range appropriate for the scattering distribution examined. Typical camera lengths are between 1 and 3 m, giving a range of scattering vector Q between 0.01 and 0.2 Å^{-1} (where the scattering vector $Q = 4\pi/\lambda \sin \theta/2$ for a scattering angle θ) at the longer camera length and between 0.04 and 0.7 Å^{-1} for the shorter camera. Standard data reduction, involving transmission correction and removal of the background scattering, was carried out before data fitting could progress. In the case of shorter camera lengths, a correction to take account of *slit smearing*[12] must be considered. Subtraction of the scattering due to the mylar substrate is of self-evident importance, particularly given the fact that there can be an orientational variation in its otherwise smooth scattering profile. In these experiments care was taken to use a section of mylar that had been shadowed from the depositing plasma, and to maintain the mylar/sample orientation between pairs of scans.

IV. PHASE SEPARATION

A. The scattering peak

For a phase-separated material in which small semiconductor$_x$ metal$_{1-x}$ regions exist within a semiconductor matrix, the properties of, and correlations between the alloyed areas result in an electron density contrast, which in turn gives rise to small-angle scattering (SAXS). The observed SAXS profile would then consist of a main scattering peak whose intensity, width, decay, and position in Q-space depend on the properties of the separated areas, in particular the position and width depend on real-space parameters (size/correlation length and the associated spread) while the peak height will depend on the scattering contrast and the number of scatterers. However, the presence of voids will have

analogous effects on the scattering profile, so any interpretation of the data must include discussion of this point.

Papers describing the phase behavior of a dynamic multicomponent mixture have used several models to describe the scattering resulting from medium range correlations, for example, the Landau theory for phase separation[13] of Cahn's linear theory of spinodal composition.[14] Teubner and Strey[13] use the Cahn–Hilliard formulation[15,16] with the Landau free energy[17] to devise a formula for the scattered intensity from a dynamic phase separated medium. Li and Ross[14] again use the Cahn–Hilliard model, this time to study the arrangement of pores within porous Vycor glass.

In a strict sense, however, the two methods above are valid only for a *dynamic* system, i.e., one in which the phase separated system is fluctuating as a function of time, and not for a system which has undergone phase separation but is now stable. Indeed, attempting to fit the data in an empirical fashion using the functional forms that arise from these approaches failed, although peak positions can be fitted, the associated model peak shapes did not match the data over more than a narrow Q-range.

In the absence of a theory which describes or models the experimental data, it is necessary to interpret the freely available parameters of the scattering distributions, such as peak position, peak width, etc., in order to obtain real-space information. This approach allows us to determine various properties of the scattering inhomogeneities while their source remains ambiguous.

B. Aggregation

In some cases the aggregation or clustering of phase-separated areas can become part of or be connected via a network; this network can display "fractal-like" properties[19] at long length scales. In addition to the main scattering peak, therefore, additional information can be obtained from the lower-Q data, resulting from larger sized correlations within the material. In particular, there are two types of fractalinity which may be present; aggregation effects can result in a clustering of segregated regions such that the distribution of mass of scatterers within a sphere of certain radius displays self-similarity; alternatively the surface of a scattering object may display surface roughness such that the surface area within a certain radius displays self-similarity over a range of length scales. If the dimension over which the cluster exists is large compared to the size of the individual units within it, then the intensity profile can be approximated to a very simple power-law relationship[20,21] $I(Q) \sim Q^{-D_m}$, where D_m is the mass fractal dimension which may have values between 1 and 3 according to the increasing densification of the medium. Alternatively, the scattering may be influenced by surface texture of the inhomogeneity, which gives rise to the relation[22] $I(Q) \sim Q^{-(6-D_s)}$, where D_s is the surface fractal dimension, which has a value of 2 for a smooth surface and rises toward 3 as the surface becomes rougher. A fractal relation is recognized by a linear region on a log $[I(Q)]$ versus log Q plot, but it is important to check that a sufficient range is covered since many functions exhibit approximate linearity over restricted length scales and it seems that a range of a decade or more in Q is required before significance can be attributed to the relationship. At sufficiently high Q, any scattering distribution from a sample with a sharp interface between regions of varying electron density will approach the asymptotic region equivalent to smooth pores where the Porod law[12] applies, i.e., $I(Q) \sim Q^{-4}$. Any small deviations away from this value, which do not correspond to surface roughness, may indicate a diffuse surface or surface curvature between the areas of differing electron density. Ding and Anderson[23] conducted molecular dynamics simulations of the structure of molybdenum within an amorphous germanium random network, i.e., a-Ge$_x$Mo$_{1-x}$. They noticed that the Mo atoms did not substitute for Ge atoms at low metal concentrations, but tended to cluster and form chains or rings which distort the local Ge random network. The small angle scattering from such a system would produce the fractal-like behavior indicated above, with a mass fractal dimension dependent on the density of the chains or clusters.

Scattering from phase-separated regions and that resulting from a fractal network, if present, may be added with appropriate weighting factors to produce a total scattering pattern. In addition, a small amount of underlying scattering may be present if there are a large number of pores (voids) with sizes in the region of a few nanometers. There is often an ambiguity in the interpretation of small angle scattering data, which is due to the various physical phenomena which can give rise to an electron density contrast and therefore small angle scattering, e.g., voids, chemical inhomogeneities, defects, etc. Using anomalous small angle scattering (ASAXS) at the molybdenum absorption edge, Regan and Bienenstock[24,25] have studied a-Ge$_x$Mo$_{1-x}$ and have been able to eliminate ambiguities in the origin of the scattering peak. They conclusively state that the chemical inhomogeneities observed in their films result from the nonrandom distribution of molybdenum within the germanium network; this lends additional support to our interpretation and conclusions presented below.

V. SAXS RESULTS AND DISCUSSION

A. a–Si$_x$Sn1$-x$:H

Three amorphous hydrogenated silicon$_x$tin$_{1-x}$ films with nickel concentrations between 3.8 and 12.5 at.%

were examined at a SAXS camera length of 2 m; this arrangement provides a Q range of ~ 0.02 to 0.35 Å^{-1}. The expectation is that the incorporation of the group IV element tin into a silicon (or germanium) TRN will be different from that of a $4/5d$ series metal on the atomic scale. The α and β phase crystalline structure of tin clearly delineate it from the transition/noble metals; the α phase is a "zero-gap semi-conductor".[26] It is therefore no surprise to observe in Fig. 2 the lack of any significant SAXS intensity above background levels. We may therefore conclude that the Sn has indeed been incorporated, with tetrahedral coordination, in a random substitutional manner. Further, if we assume that, irrespective of the metal incorporated, the void content of the native a-Si:H network will be similar from sample to sample, then we may conclude from this data that the void scattering is not a significant factor and may be ignored in this Q range.

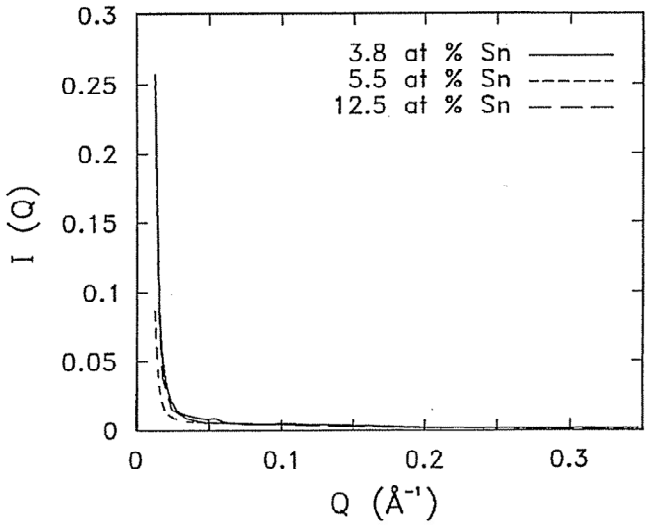

FIG. 2. Scattering from a-Si$_x$Sn$_{1-x}$:H at various tin concentrations; the $I(Q)$ scale is relative, not absolute.

B. a–Ge$_x$Au1$-x$

Six rf sputtered amorphous thin films with concentrations of gold between 9.6 and 31.2 at.% were examined at a SAXS camera length of 2.5 m; this arrangement provides a Q range of ~ 0.008 to 0.20 Å^{-1}. Figure 3 shows the scattering data from the a-Ge$_x$Au$_{1-x}$ films with varying gold concentration. Although there are some anomalies in the shape of the curves, a general trend is discernible with the scattering peak becoming more defined and moving to lower Q values with increasing gold content. In addition, for gold concentrations above 20 at.% a second peak is observed at lower Q which becomes stronger until it dominates the scattering at concentrations over 30 at.%. Table I shows the position of the scattering peak(s) in Q space averaged over several repeat measurements, and gives an indication of the mean FWHM for each peak. In addition, the fitted "fractal dimension" resulting from a naïve fit to the low-Q data is provided where possible (note, however, that these dimensionalities should be treated with due caution given the limited Q-range over which the data can be fitted).

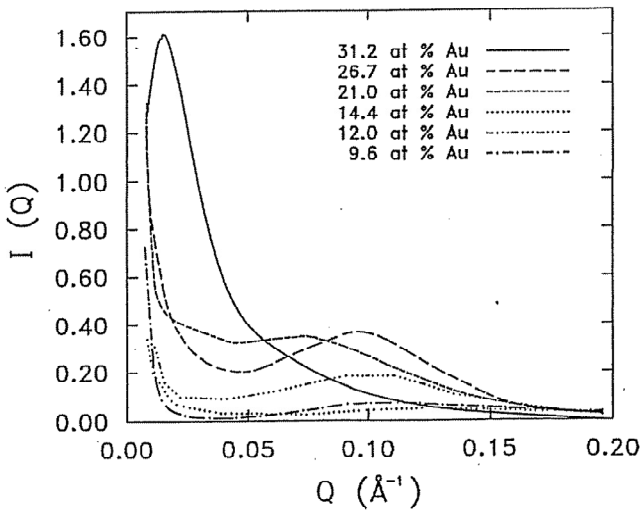

FIG. 3. Scattering from a-Ge$_x$Au$_{1-x}$ at various gold concentrations; the $I(Q)$ scale is relative, not absolute.

TABLE I. Fitted parameters for the a-Ge$_x$Au$_{1-x}$ samples.

at.% Au	"fractal dimension" $D_m \pm 0.05$	Q_{max} ±0.01 Å^{-1}	approx. FWHM (Å^{-1})	Q_{max} ±0.01 Å^{-1}	approx. FWHM (Å^{-1})
9.6	3.0	0.115	0.077	...	...
12.0	2.95	0.094	0.054	...	...
14.4	2.70	0.128	0.061	...	...
21.0	2.95	0.072	0.071	0.022	0.03
26.7	1.80	0.092	0.063	...	...
31.2	...	0.054	0.057	0.016	0.023

While Q_{max} for the peak generally becomes lower with increasing gold content, indicating that the correlation length associated with segregated areas is increasing (from ~ 50 to ~ 100 Å), the width of the peak remains stable at ~ 0.06 Å^{-1} (corresponding to variations in size of ±25 Å) for all samples. There are, however, some scattering curves which do not follow this trend, particularly those from the 14.4 and 26.7 at.% Au samples. This might be explained by variations in composition across a given film.

The increase in the distance between scattering centers (i.e., the segregated regions within the film) with increasing gold content suggests that the alloyed regions are closely packed in groups throughout the film, so that

an increase in gold produces larger segregated volumes, which, for an equivalent packing fraction, increases the distance between alloy centers. If the alloyed volumes were distributed randomly throughout the film then the distance between their centers would either decrease or stay the same when the gold concentration is increased (the clustering actually evidenced here may account for the observation that the scattering from different parts of the film can vary considerably, and hence may be why two of the lower Au concentration films have parameters which appear out of sequence).

In general, the peak height, as seen in Fig. 3, increases with composition as the peak moves into lower Q values. If one now recalls that the illuminated volume of sample is approximately the same in all cases, then, on a simplistic level, this increase in scattering contrast suggests that there are more scattering centers in the higher concentration samples (i.e., consistent with the increased amount of gold present).

At gold concentrations above 20 at.%, a second scattering peak appears at a low Q value of ~ 0.03 Å^{-1} (200 Å) which increases in intensity and dominates the scattering at gold concentrations over 30 at.%. This peak is thought to result from areas of metallic gold which are embedded in the germanium network, as predicted by EXAFS results and supported by x-ray diffraction.[8]

The lower-Q region of the a-Ge$_x$Au$_{1-x}$ scattering data shows a sharp increase in intensity, above the background scattering, which can be analyzed, with caution, in terms of the scattering from a self-similar structure. Table I shows the gradients of the low-Q part of the plot, which is equivalent to the "mass fractal dimension" of the fractal network (if indeed that is an appropriate description). There is a slight and gradual decrease in D_m from 3 at the lowest gold concentration. (A fractal dimension of 3 means that the volume of scatterers scales with the cube of the distance, and is therefore consistent with a random arrangement of scattering centers. As D_m decreases the scattering results from a more correlated structure as shown schematically in Fig. 4, until for relatively low D_m the structure is open and branched. This kind of behavior has been predicted by MD simulation for a-Mo$_x$Ge films.[23])

C. a-Si$_x$Ni1$-x$: H

Six amorphous hydrogenated silicon$_x$nickel$_{1-x}$ films with nickel concentrations between 3.5 and 29 at.% were examined at a SAXS camera length of 1 m; this arrangement provides a Q range of ~ 0.04 to 0.7 Å^{-1}. The samples were also studied at longer camera lengths, but no additional information was revealed; data are not presented here.

Figure 5 shows scattering from the six a-Si$_x$Ni$_{1-x}$: H films. All the data show a scattering peak on a flat background, with little intensity at lower Q values. Table II details the peak position and FWHM derived from the scattering.

There is a general increase in scattering intensity with increasing nickel content, and the peak width de-

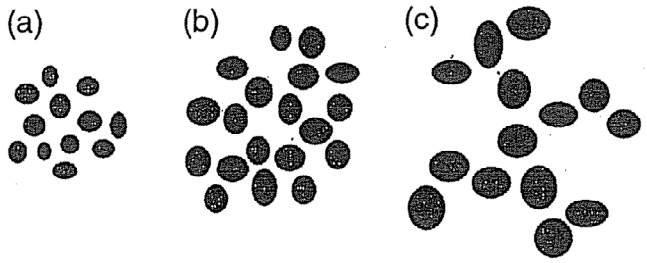

FIG. 4. A possible physical interpretation of the scattering data from a-Ge$_x$Au$_{1-x}$: (a) low Au content, small alloyed volumes with $D_m = 3$; random arrangement of scattering centers; (b) intermediate Au content, larger alloyed volumes with $D_m \sim 2.9$; some correlation between scattering centers; (c) high Au content, large alloyed volumes with $D_m \sim 2$; correlated scattered centers forming a mesoscopic network.

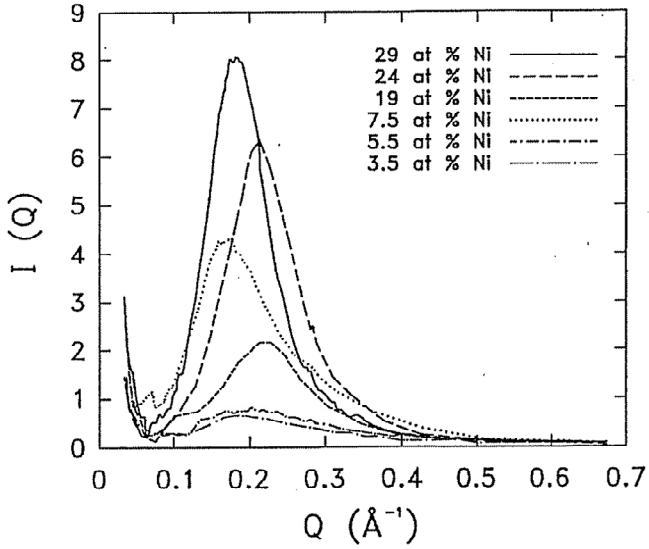

FIG. 5. Scattering from a-Si$_x$Ni$_{1-x}$: H at various nickel concentrations; the $I(Q)$ scale is relative, not absolute.

TABLE II. Fitted parameters for the a-Si$_x$Ni$_{1-x}$: H samples.

at.% Au	Q_{max} ±0.005 Å^{-1}	FWHM (Å^{-1})
3.5	0.20	0.146
5.5	0.195	0.120
7.5	0.17	0.110
19.0	0.22	0.110
24.0	0.22	0.105
29.0	0.185	0.095

creases slightly, suggesting that there is less spread in the correlation distances between nickel silicide scattering centers. The variation of this parameter between samples is small (corresponding to a change in size from 30 to 40 Å). Figure 6 shows the variation in Q_{max} and FWHM of the scattering peaks for the a-Ge_xAu_{1-x} and a-Si_xNi_{1-x}:H samples. However, although the shifts in peak position (and therefore correlation length in real-space) are significantly larger than the fit errors and were reproducible, we are unable to discern a simple physical explanation for them. It is presumably related to the detailed nature of the formation of nickel silicide (or gold-germanium alloy, and gold) volume elements and their mutual coalescence/segregation within the native TRN. As the metal concentrations increase, the small clusters grow (either through metal diffusion/aggregation or cluster coalescence); the energetics of this phase separation process will tend also to favor a well-defined TRN/cluster boundary. The result of these processes will be progressive competition between the separation of the clusters and the energy advantage of their coalescence as they grow. At a sufficiently high metal content (which will be less than 50 at.% due to the Si, or Ge, content of the cluster itself), the SAXS profile will begin to reflect the correlations between the TRN volume elements rather than the semimetallic alloy volume elements. Little very-low angle scattering intensity was observed in the a-Si_xNi_{1-x}:H samples. This would indicate that there is limited aggregation of nickel silicide regions (e.g., into fractal-like regions) or that the regions are distributed randomly.

VI. CONCLUSIONS

The SAXS data presented here demonstrates the accuracy of earlier EXAFS-based suggestions that transition/noble metals are *not* incorporated in a simple, random substitutional, fashion into a native TRN such as a-Si:H and a-Ge. This leads us to confirm our earlier statement that a volume percolation model is more appropriate than the "homogeneous" Anderson transition model as an explanation for the observed MIT transition. These conclusions are not model-dependent since they rely solely on peak positions and associated FWHM values. Further, the data reveal the overall cluster growth as well as a clear indication of cluster correlation/ordering within one of the systems studied (a-Ge_xAu_{1-x}). As anticipated, the model a-Si_xSn_{1-x}:H system showed no signs of cluster formation or other heterogeneities (e.g., voids) on the length scales probed.

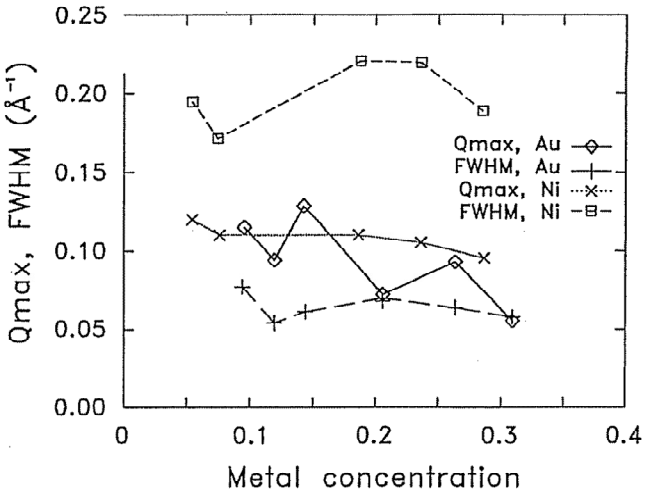

FIG. 6. Variation in Q_{max} and FWHM of the scattering peaks for the a-Ge_xAu_{1-x} and a-Si_xNi_{1-x}:H samples.

ACKNOWLEDGMENTS

The authors would like to acknowledge the help given by the staff of the CCRL Daresbury Laboratory, particularly W. Bras; E. A. Davis kindly allowed his sputtering equipment to be used for the sample deposition, which was undertaken by A. M. Edwards. We wish to record our gratitude to S. J. Gurman, who has taken a keen interest in the data and has freely discussed its interpretation with us, and to A. N. North for guidance in the early stages of the experimental SAXS work. Rutherford Backscattering measurements were undertaken by C. Jeynes of the University of Surrey Ion Beam Centre. The work was funded by the EPSRC and the University of Kent at Canterbury.

REFERENCES

1. K. Morigaki, Philos. Mag, B **42**, 979 (1980).
2. R. Zallen and H. Scher, Phys. Rev. B **4**, 4471 (1971).
3. H. Itozaki, N. Fujita, T. Igarishi, and H. Hitotsuyanagi, J. Non-Cryst. Solids **50/60**, 589 (1983).
4. A. Mahan, D. L. Williamson, and A. Madan, Appl. Phys. Lett. **44**, 220 (1984).
5. A. M. Edwards, M. C. Fairbanks, R. J. Newport, S. J. Gurman, and E. A. Davis, J. Non-Cryst. Solids **113**, 41 (1989).
6. A. M. Edwards, M. C. Fairbanks, and R. J. Newport, Philos. Mag. **63B**, 437 (1991).
7. A. M. Edwards, M. C. Fairbanks, and R. J. Newport, Physica B **167**, 247 (1990).
8. A. M. Edwards, M. C. Fairbanks, R. J. Newport, and S. J. Gurman, Vacuum **41**, 1335 (1990).
9. A. M. Edwards, S. J. Gurman, M. C. Fairbanks, and R. J. Newport, in *X-ray Absorption Fine Structure*, edited by S. S. Hasnain (Proc. XAFS VI, Ellis Horwood, London, 1991), p. 294.
10. K. M. Abkemeier, C. J. Adkins, R. Asal, and E. A. Davis, J. Phys.: Cond. Matt. **4**, 9113 (1992), and other references therein.
11. R. Asal, S. H. Baker, S. J. Gurman, S. C. Bayliss, and E. A. Davis, J. Phys.: Cond. Matt. **4**, 7169 (1992).
12. O. Glatter and O. Kratky, *Small-Angle X-ray Scattering* (Academic Press, New York, 1982).
13. M. Teubner and R. Strey, J. Chem. Phys. **87**, 3195 (1987).
14. J. C. Li and D. K. Ross, J. Phys.: Cond. Matt. **6**, 351 (1994).
15. J. W. Cahn and J. E. Hilliard, J. Chem. Phys. **28**, 258 (1958).
16. J. W. Cahn, J. Chem. Phys. **42**, 93 (1965).
17. L. D. Landau and E. M. Lifscitz, *Statische Physik* (Akademie, Berlin, 1979).

18. S. R. Elliot, Adv. Phys. **38**, 1 (1989).
19. D. Avnir, *The Fractal Approach to Heterogeneous Chemistry* (John Wiley & Sons, New York, 1989).
20. J. Teixeira, J. Appl. Crystallogr. **21**, 781 (1988).
21. P. W. Schmidt, J. Appl. Crystallogr. **24**, 414 (1991).
22. P. W. Schmidt, D. Avnir, D. Levy, A. Hohr, M. Steiner, and A. Roll, J. Chem. Phys. **94**, 1474 (1991).
23. K. Ding and H. C. Anderson, Phys. Rev. B **36**, 2675 (1987).
24. M. J. Regan and A. Bienenstock, J. Non-Cryst. Solids **192 & 193**, 644 (1995).
25. M. J. Regan and A. Bienenstock, Phys. Rev. B **51**, 12 170 (1995).
26. S. H. Groves and W. Paul, Phys. Rev. Lett. **11**, 194 (1963).